Fluorescence-aided Tomographic Imaging of Synovitis in the Human Finger[1]

Pouyan Mohajerani, MS
Maximilian Koch, MS
Klaus Thürmel, MD
Bernhard Haller, MS
Ernst J. Rummeny, MD
Vasilis Ntziachristos, PhD
Reinhard Meier, MD

Purpose: To propose and evaluate indocyanine green (ICG)–enhanced tomographic optical imaging for detection and characterization of synovitis in affected finger joints of patients with rheumatoid arthritis and differentiation from healthy joints in comparison to 3-T magnetic resonance (MR) imaging.

Materials and Methods: This prospective pilot study was approved by the institutional ethics committee. Six arthritic proximal interphalangeal (PIP) joints in six patients (five women and one man; mean age ± standard deviation, 62.6 years ± 13.3) with clinically determined rheumatoid arthritis and six healthy PIP joints from six volunteers (four women and two men; mean age, 41.5 years ± 20.2) were examined with an ICG-enhanced fluorescence molecular tomography (FMT) system and 3-T MR imaging as the standard of reference. The degree of inflammation was graded semiquantitatively on a four-point ordinate scale according to the Outcome Measures in Rheumatology Clinical Trials Rheumatoid Arthritis MR Imaging Score, or OMERACT RAMRIS. FMT reconstructions were coregistered with the MR images. Groups were compared by using a two-sided *t* test, and a weighted κ coefficient was used for comparing FMT and MR imaging semiquantitative scores, as well as assessing intrareader agreement.

Results: FMT was used to detect synovitis in all arthritic joints. The reconstructed FMT signal correlated with MR imaging findings in intensity and spatial, transverse profile. Semiquantitative scoring of FMT correlated well with MR imaging findings (weighted κ coefficient = 0.90). The reconstructed quantitative FMT signal, denoting synovial hyperperfusion, was used to differentiate between synovitis and healthy joints (healthy joints, 1.25 ± 0.59; arthritic joints, 3.13 ± 1.03; $P < .001$).

Conclusion: FMT enhanced with ICG provided depth-resolved imaging of synovitis in PIP joints. FMT may help detect synovitis in patients with rheumatoid arthritis.

Online supplemental material is available for this article.

[1] From the Institute for Biological and Medical Imaging, Technische Universität München and Helmholtz Zentrum München, Ingolstädter Landstrasse 1, Neuherberg 85764, Germany (P.M., M.K., V.N.); and Department of Rheumatology (K.T.), Institute for Medical Statistics and Epidemiology (B.H.), and Department of Radiology (E.J.R., R.M.), Klinikum rechts der Isar, Technische Universität München, Munich, Germany. Received September 18, 2013; revision requested October 29; revision received January 31, 2014; accepted March 17; final version accepted March 21. **Address correspondence to** P.M. (e-mail: *pouyan.mohajerani@gmail.com*).

Rheumatoid arthritis (RA) is an inflammatory disorder characterized by inflammation of the synovial lining of joints (synovitis) and subsequent destruction of the joint. Detection and assessment of disease progression in RA are based on a combination of clinical, laboratory, and imaging data. Since early initiation of effective therapy prevents destruction, preserves function, and is able to induce lasting remission, there is a demand for sensitive and specific imaging tools to detect synovitis as an early marker of RA (1). Radiography is commonly used clinically; however, it will only show changes after months or years of active disease (2). Ultrasonography and magnetic resonance (MR) imaging display improved diagnostic capabilities; however, they show varying interoperator variability and high costs, respectively (3).

Optical imaging has also been considered for imaging arthritis in human finger joints (4–9). Optical methods operate with nonionizing radiation and are well suited for the finger dimensions that are typically affected by RA. Therefore, optical methods can play an important role in the clinical management of disease if they could be shown to offer accurate diagnostic performance. Transillumination planar imaging (10) and tomographic approaches (5,11,12) have been proposed, making use of changes in the optical absorption and scattering coefficients of affected tissue in finger joints. These methods can be used to differentiate between healthy and arthritic joints fairly successfully when the optical properties have substantially changed owing to clouding of synovial fluid or membrane (10). We have also previously used indocyanine green (ICG), a nonspecific, clinically approved synthetic organic near-infrared fluorescent dye, in the detection of inflammatory lesions in hand joints by using planar fluorescence imaging (4,8). However, planar imaging methods do not resolve information with depth and instead deliver a weighted projection of the underlying three-dimensional fluorophore distribution (13), thus limiting sensitive and quantitative detection of synovitis (4). Fluorescence molecular tomography (FMT) has been proposed as a noninvasive modality for quantitative three-dimensional imaging of fluorescence in vivo, allowing reconstruction of the true underlying probe biodistribution by modeling diffuse propagation of light (14). ICG has been previously applied in conjunction with other tomographic imaging approaches for clinical applications (15–19) and several preclinical applications (20–24).

The clinical utility of FMT for three-dimensional imaging of synovitis in the human finger joint, however, has not been well established in the literature. The purpose of our pilot study was to propose and evaluate ICG-enhanced FMT for in vivo detection and characterization of synovitis in finger joints of patients with RA and differentiation from healthy joints, in comparison to MR imaging findings.

Advances in Knowledge

- Acquisition, processing, and inversion methods were optimized for a 360° fluorescence molecular tomography (FMT) system for in vivo indocyanine green–enhanced imaging of human finger joints.
- FMT demonstrates healthy and arthritic joints according to reconstructed signal intensity (mean ± standard deviation for volunteers, 1.25 ± 0.59; for patients, 3.13 ± 1.03; $P < .001$).
- The reconstructed fluorescence signal has a spatial intensity profile similar to that of MR imaging.

Implication for Patient Care

- FMT allows for detection and characterization of synovitis in finger joints of patients with rheumatoid arthritis; because of its high sensitivity, FMT is a potential complementary imaging tool for early detection of inflammation.

Materials and Methods

Our study was approved by the ethics committee at our institution before its commencement; it was conducted according to the principles of the Declaration of Helsinki, and all patients provided written informed consent before participating in the study.

Patients and Clinical Examination

Twelve study participants, consisting of six patients with RA (five women and one man; mean age, 62.6 years ± 13.3) and six volunteers (four women and two men; mean age, 41.5 years ± 20.2) were included in this prospective study and were recruited from March 2012 to November 2013 through the Department of Rheumatology at Klinikum rechts der Isar, Technical University Munich. Inclusion criteria for the patients were tender and/or swollen joint(s) of the proximal interphalangeal (PIP) joint of the examined second or third index finger, clinically determined RA, and willingness to participate. Inclusion criteria for the volunteers of the control group were no tenderness or swelling in a healthy PIP joint and a willingness to participate. Exclusion criteria were pregnancy; renal failure; known allergy to iodine, ICG, or gadolinium-based contrast agent; and other

Published online before print
10.1148/radiol.14132128 **Content codes:** MK MI

Radiology 2014; 272:865–874

Abbreviations:
FMT = fluorescence molecular tomography
ICG = indocyanine green
MIP = maximum intensity projection
PIP = proximal interphalangeal
RA = rheumatoid arthritis
ROI = region of interest

Author contributions:
Guarantors of integrity of entire study, P.M., V.N., R.M.; study concepts/study design or data acquisition or data analysis/interpretation, all authors; manuscript drafting or manuscript revision for important intellectual content, all authors; approval of final version of submitted manuscript, all authors; literature research, P.M., K.T., R.M.; clinical studies, K.T., E.J.R., R.M.; experimental studies, P.M., M.K.; statistical analysis, P.M., M.K., B.H., R.M.; and manuscript editing, P.M., M.K., K.T., E.J.R., V.N., R.M.

Conflicts of interest are listed at the end of this article.

contraindications to MR imaging, such as metallic fragments in the body, magnetically activated implanted devices, and claustrophobia. Clinical work-up was performed by a rheumatologist (K.T.), including bimanual palpation and laboratory tests.

MR Imaging

The patients underwent 3-T MR imaging (Verio; Siemens, Erlangen, Germany) by using a flexible surface coil at the Department of Radiology of Klinikum rechts der Isar, Technical University Munich. T1-weighted fat-saturated contrast material–enhanced MR images were obtained with patients in the prone position, and the hands were outstretched in a praying position to image both hands at once. The protocol used is presented in Appendix E1 (online). The degree of synovitis in the PIP joint on MR images was graded semiquantitatively by a radiologist (R.M., with 6 years of experience in musculoskeletal MR imaging). A repeated interpretation of the MR images 2 weeks after the first was performed by one reader (R.M.), with rearrangement of the image sets for intrareader agreement estimation. The reader scored the images without having knowledge of the clinical assessment and was blinded to patient name and results of FMT. MR images were evaluated in random order by using the semiquantitative assessment system suggested by the Outcome Measures in Rheumatology Clinical Trials, or OMERACT, MR imaging group (25). With this method, synovitis is scored on a scale of 0 to 3 for each joint, with 0 representing no synovitis and 1 to 3 representing mild, moderate, and severe arthritis, respectively.

FMT Acquisition System and Method

A 360°-rotation FMT system located and designed at the Institute for Biologic and Medical Imaging at the Helmholtz Zentrum München, Munich, Germany (26), shown in Figure 1, was used for imaging the PIP joint–a joint commonly affected in RA. The imaging protocol was optimized to allow acquisition over several hundred source positions with reasonable signal quality and imaging time. Further details regarding the acquisition method are presented in Appendix E2 (online).

The FMT measurements and processing were performed after MR imaging, and readers were not blinded to MR images. The tip of the finger was placed in a thimble, which serves as a reference pivotal point. Laser scanning was performed within a field of view of around 15 mm in the axial direction, centered on the region of interest (ROI) at 17 equally spaced gantry angles. A 750-nm laser (B&W Tek, Newark, Del) was used to scan the sample at a mean of 15 source locations per gantry angle, where, at each location, intrinsic and fluorescence images were obtained by using a cooled charge-coupled device camera (Pixis 512B; Princeton Instruments, Trenton, NJ). The imaging consisted of acquisition of front-illumination images at every 10° (used for volume reconstruction) during the first minute of imaging (exceptions presented in Appendix E2 [online]).

FMT was planned 20 minutes after intravenous bolus injection of 1 mg of ICG per kilogram of body weight (actual imaging time was 21.6 minutes ± 5.6, Table). Patients placed the hand inside the FMT device on an armrest in the prone position. Imaging lasted a mean of 12 minutes (11.8 minutes ± 2.2). Motion was compensated for during both acquisition and reconstruction. Front-illumination images were used to reconstruct a three-dimensional volume of the imaged tissue, which was required for modeling the light propagation and as a geometric reference for motion compensation (Appendix E2 [online]). Light propagation in the finger tissue was modeled by using finite

Figure 1

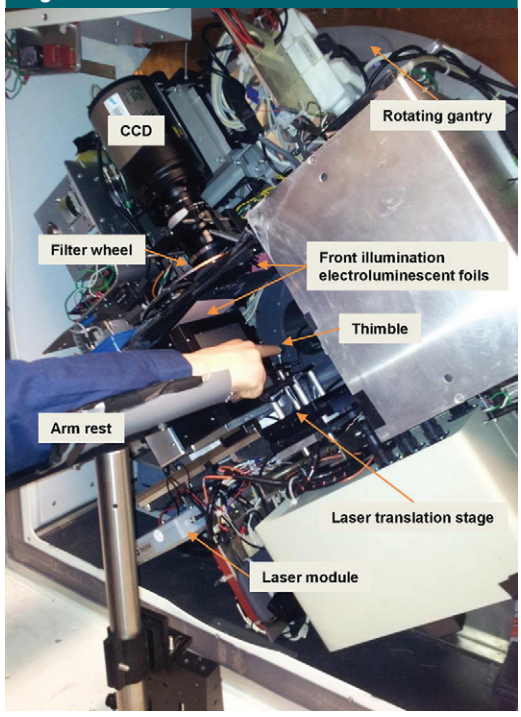

Figure 1: Photograph of the FMT system for imaging human finger joints. The 360°-rotation FMT system is shown with the optical components and the hand on a holder in prone position with the second (index) PIP joint stretched out. The front face of the system is covered with a lead plate that has a hole in the middle, allowing for hand placement in the imaging chamber. *CCD* = charge-coupled device.

Experimental and Processing Details for Individual Volunteers and Patients

Study Participant No.	Age (y)	Sex	Joint*	MR Imaging Score, First Reading	MR Imaging Score, Second Reading	FMT Score	Time Point†	Imaging Length (min)	Mean Signal Intensity Value	Maximum Signal Intensity Value	Root Mean Square Signal Intensity Value
1 (Volunteer)	27.6	Male	Second right	0	0	0	23	11	1.67	3.79	1.76
2 (Volunteer)	33.6	Male	Third left	0	0	0	14	12	0.72	1.49	0.76
3 (Volunteer)	28.5	Female	Second right	0	0	0	16	8	1.40	2.84	1.48
4 (Volunteer)	25.4	Female	Second right	0	0	0	27	8	1.44	3.39	1.51
5 (Volunteer)	61.2	Female	Second right	0	0	0	18	11	1.24	2.38	1.30
6 (Volunteer)	72.8	Female	Third right	0	0	0	18	11	1.00	1.85	1.04
7 (Patient)	66.7	Female	Second right	2	2	2	33	12	2.44	5.39	2.58
8 (Patient)	41.3	Female	Third left	2	2	3	24	13	4.25	8.62	4.49
9 (Patient)	72.2	Female	Third left	3	2	2	20	13	2.41	5.28	2.56
10 (Patient)	66.6	Female	Third right	3	3	3	20	13	2.91	8.05	3.04
11 (Patient)	76.	Female	Third right	3	3	3	28	13	3.56	7.57	3.73
12 (Patient)	52.2	Male	Third left	3	3	3	18	16	3.19	7.46	3.33

* Second and third joints denote PIP joints of the index and middle fingers, respectively.

† The imaging time point designates the start of the FMT acquisition after intravenous ICG administration.

element method–based discretization of the diffusion equation (27).

FMT Processing

A flowchart of FMT processing is presented in Figure E1 (online). The same processing parameters were applied to all study participants. The three-dimensional volume that designated the tissue volume was reconstructed by using the 34 front-illumination images by means of back-projection of the image boundaries based on the geometric description of the camera (Appendix E2 [online]). Homogeneous optical absorption and scattering were used in the FEM-based modeling of light propagation in the finger. Finger motion in the transverse plane was corrected by finding the offset between the acquired intrinsic images and the projection of the three-dimensional volume for the given gantry angle. The intrinsic and fluorescence images were then optimally shifted to match the projected image of the volume, and source position locations were corrected accordingly. This scheme can compensate for translational motion in the transverse plane, but not motion in the axial direction or rotation of the finger. Further details regarding FMT processing are presented in Appendix E2 (online).

Furthermore, the fluorescence signal intensity was observed to decrease exponentially with a half-time of 13 minutes (Appendix E2 [online]). To compensate for ICG fluorescence decay, the measured fluorescence images were correspondingly weighted prior to reconstruction, based on their acquisition time point (with the 20-minute postinjection time point taken as the zero time point, Appendix E2 [online]). This operation also compensated for differences between the actual imaging times (21.6 minutes ± 5.6, Table) and the planned 20-minute postinjection time point. These time differences were unavoidable owing to logistical limitations, such as hardware or experiment interruptions or the study participant's preference for speedier completion.

A background subtraction method based on the approach described (28) was applied to normalized Born data (defined as the ratio of the fluorescence to the intrinsic signal) to compensate for nonspecific uptake of ICG (Appendix E2 [online]). Reconstruction was performed with 1-mm^3 spatial resolution by using the least-squares method (29).

Palmar creases were used as anatomic surface markers and were indicative of the underlying joint location (30). The reconstructed FMT signal was limited to a ROI with a span of 2 mm distal from the crease location (Appendix E2 [online]) and 3 mm proximal to it. A maximum intensity projection (MIP) of the fluorescence signal within this ROI, called the MIP ROI, was coregistered with the MR image (Appendix E2 [online]). Reconstruction was performed with an "imaging ROI," which consists of a spatial span along the axial direction scanned by the virtual optical detectors.

Moreover, the FMT reconstruction results can be scored from 0 to 3 according to the intensity in a fashion similar to MR imaging. FMT reconstructions were scored semiquantitatively according to the mean intensity. Two threshold values, μ_1 and μ_2, were used. FMT signal intensity values (averaged signal intensity within the MIP ROI) less than μ_1 were assigned a semiquantitative score of 0, while values between μ_1 and μ_2 were considered to indicate moderate synovitis and were given a score of 2. Values larger than μ_2 were assigned a score of 3–indicating severe synovitis. The thresholds μ_1 and μ_2 were set according to the collection of signal intensity values measured for the 12 subjects in our study.

Statistical Analysis

A two-sample *t* test was used to compare the mean values of the FMT reconstructed signals within an axial field of view 5 mm (the MIP ROI) between volunteers and patients recruited in our pilot study. The null hypothesis denoted both groups as having the same mean. A two-sided level of significance of .05 was used. With a sample size of six subjects per study group, an effect size (differences in means and standard deviations) of two can be detected with a power of 80% by using a two-sample *t* test. The correlation between the semiquantitative scoring of FMT and MR imaging was assessed by using a weighted κ coefficient (31). Correlation between semiquantitative scoring of FMT and MR imaging based on ordinal ratings (from 0 to 3) and intrareader agreement by using repeated assessments of the same images by one investigator (R.M.) was assessed by using weighted κ coefficients. The effect of the semiquantitative FMT scoring thresholds μ_1 and μ_2 on sensitivity and specificity were analyzed. Specifically, the threshold μ_1 was used to differentiate between affected (moderate and severe synovitis) and healthy joints, defined here as classification I. Sensitivity and specificity values were obtained for classification I for values of μ_1, spanning the range of measured FMT signal intensity value. Similarly, the effect of μ_2 on classification II in the differentiation between severe and nonsevere synovitis was analyzed. The Spearman rank correlation coefficient ρ was used to measure the correlation between age and FMT signal intensity values across all 12 subjects and within each group.

Results

Patients and Clinical Examination

No adverse events were seen in the study participants after intravenous injection of ICG or gadopentetate dimeglumine. Patients showed elevated parameters of serum C-reactive protein at 2.7 mg/dL (27 mg/L) and the erythrocyte sedimentation rate at 24/38 mm (1st/2nd hour), on average. For patients, the clinically most affected (swollen and tender) PIP joint of the second or third index finger was selected for the FMT imaging studies, as denoted in the Table. Volunteers did not demonstrate tenderness or swelling of the examined joints and showed normal values in the laboratory tests.

Imaging Results

FMT imaging results for a patient with moderate synovitis in the left third PIP joint are shown in Figure 2. Three-dimensional demonstration of the reconstructed FMT signal within the MIP ROI is shown in Figure 2a. MIP projection of the FMT signal in the sagittal plane is demonstrated in Figure 2b, along with the corresponding MIP and imaging ROIs. A transverse MR image of the joint is shown in Figure 2c. At MR imaging, hyperintense areas designate synovitis marked by higher uptake of the gadolinium-based contrast agent. Coregistration of the FMT MIP projection in the axial direction and the MR transverse image (Appendix E2 [online]) is shown in Figure 2d.

Figure 2e shows the location of the MR transverse section of Figure 2c on a coronal MR image and demonstrates the proximity of locations of the joint split and the palmar crease lines (see Appendix E2 [online]). FMT signal demonstrated a spatial profile similar to the MR image; increased ICG uptake is displayed mostly on the dorsal aspect, 3 mm underneath the skin with the left side (green *X*) stronger than the right side (blue *X*). These characteristics are also observed on the MR image and therefore confirm the contrast agent uptake in the inflamed synovium. The case of the second right PIP joint of a healthy joint in a volunteer is presented in Figure 3a–3c, with the MIP image normalized to the same maximum as the previous case of Figure 2. The reconstructed fluorescence for this healthy joint had the strongest signal intensity among all the six imaged healthy joints in terms of both mean and maximum intensity. FMT reconstructions for another patient are presented in Figure E6 in Appendix E3 (online). Corresponding imaging ROIs and MIP ROIs are shown in Figures 2 and 3 and Figure E6 (online).

Figure 4 shows signal intensity maximum and mean values within the reconstruction ROIs for the 12 study participants. Mean values for the FMT signal intensity (averaged within the MIP ROI) were 1.25 ± 0.59 for volunteers and 3.13 ± 1.03 for patients (P = .00015). Semiquantitative scores (scores 0–3) obtained from the FMT signal (by using the thresholds μ_1 and μ_2 shown in Figure 4a) are presented in the Table for the 12 imaged joints. The weighted κ coefficient used to quantify the association between semiquantitative scores obtained from FMT and MR imaging had a value of 0.90 for the first MR imaging reading and 0.94 for the second MR imaging reading. The effects of thresholds μ_1 and μ_2 on the sensitivity and specificity of FMT semiquantitative scores versus MR imaging scores are presented in Figure 4b and 4c. Figure 4b shows the sensitivity and specificity of the binary classification I (affected vs healthy) versus μ_1. Figure 4c presents similar results for the binary classification II (severe vs less than severe) versus μ_2.

A Spearman correlation coefficient of ρ = 0.24 was observed between the age and the FMT signal intensity values across all 12 study participants. The coefficient ρ had a value of −0.77 for the healthy group and and −0.43 for the patient group. For the intrareader agreement of repeated assessment of MR images by one reader (R.M.), a κ coefficient of 0.94 was estimated, and concordance was observed in 92% of the ratings. MR scores based on the first and second readings are presented in the Table.

Discussion

In our study, we have shown that FMT enhanced with ICG provides quantitative, depth-resolved imaging of synovitis in the PIP joint and allows differentiation between healthy and arthritic joints affected by RA, as corroborated with MR imaging. FMT

Figure 2

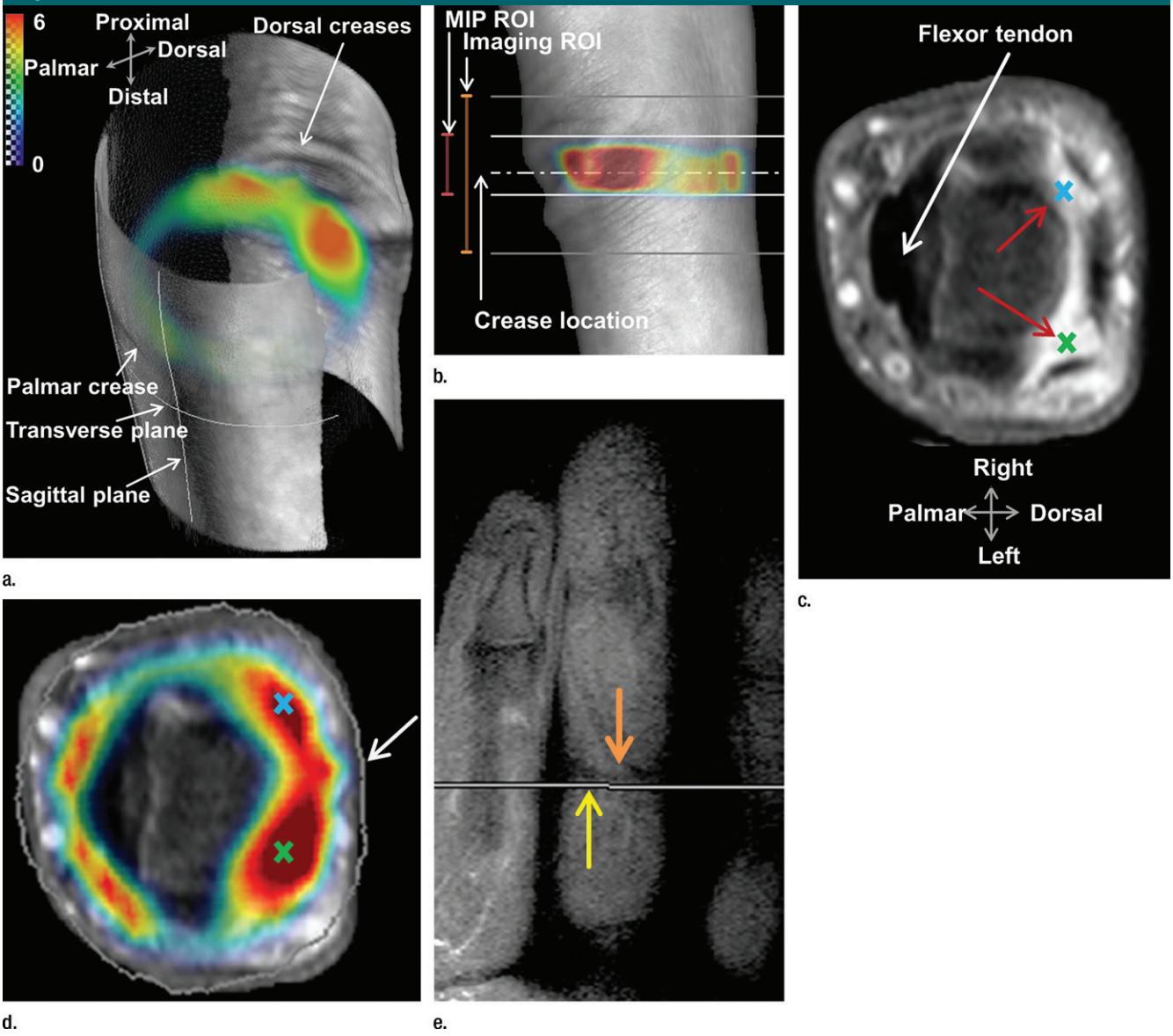

Figure 2: Images demonstrate the FMT technique. Images were acquired in the third left PIP joint (with an MR synovitis score of 2) in a 41-year-old female patient and show strong signal intensity increase (contrast enhancement) of the inflamed synovia on both FMT and MR images. **(a)** Three-dimensional representation of the reconstruction fluorescence shows where the skin photograph on the palmar and dorsal side is wrapped on the surface of the reconstructed volume. **(b)** On the sagittal MIP, the 5-mm axial ROI is shown. **(c)** On the corresponding transverse MR image, the red arrows point to the synovitis. Increased ICG uptake is displayed mostly on the dorsal aspect, 3 mm underneath the skin with the left side (green *X*) stronger than the right side (blue *X*). **(d)** On the coregistered image between the FMT MIP image and the MR transverse image, the arrow points to the boundary of the coregistered FMT volume. **(e)** On the coronal MR image, the location of the transverse image of **c** is indicated by the yellow arrow, and the orange arrow indicates the palmar creases.

signal intensities were significantly ($P < .001$) stronger for joints with moderate to severe synovitis than for healthy joints. The substantial signal intensity difference between healthy and affected joints can be explained as follows. ICG did not appear to concentrate in any specific lesion in the healthy joints and therefore contributed mainly to the background fluorescence. The background signal intensity was then substantially reduced after the background subtraction approach, leaving only weak signal components for the healthy joints in comparison to those affected by synovitis.

The FMT reconstructions in the form of MIP images closely resembled

Figure 3

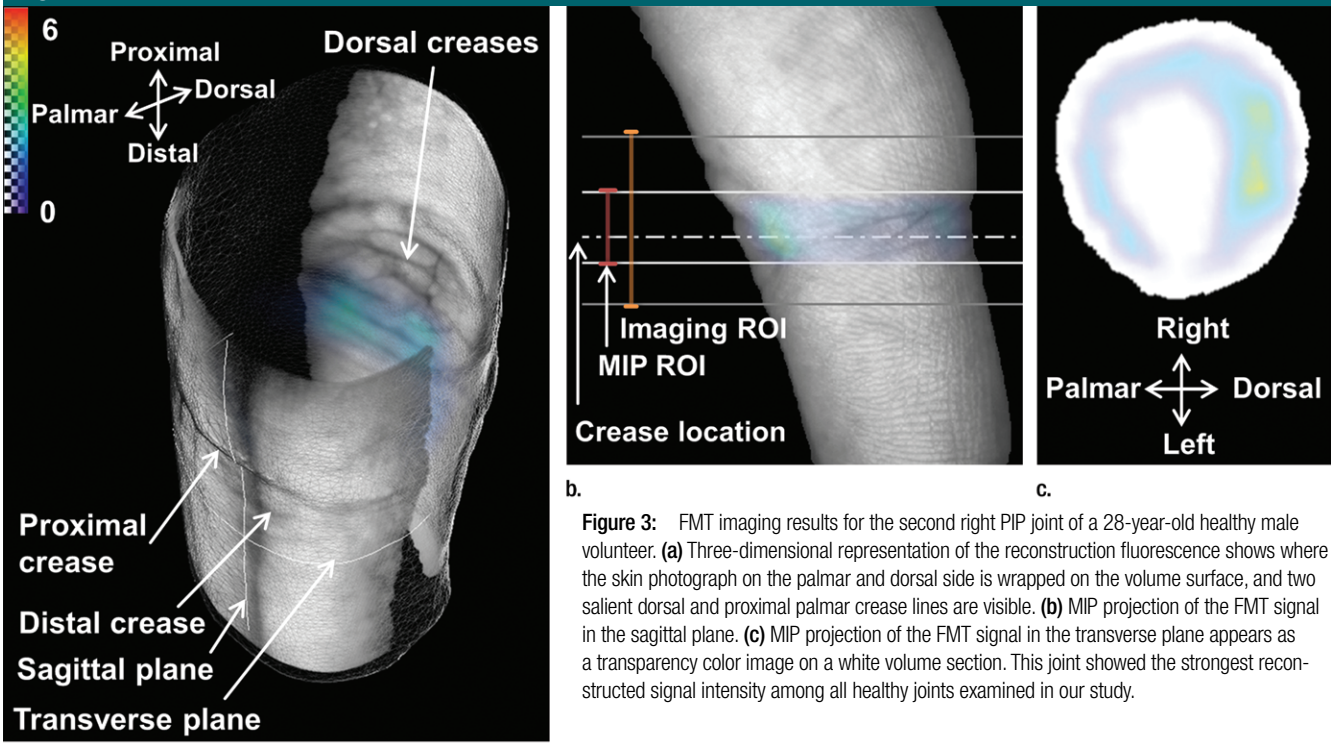

a. b. c.

Figure 3: FMT imaging results for the second right PIP joint of a 28-year-old healthy male volunteer. **(a)** Three-dimensional representation of the reconstruction fluorescence shows where the skin photograph on the palmar and dorsal side is wrapped on the volume surface, and two salient dorsal and proximal palmar crease lines are visible. **(b)** MIP projection of the FMT signal in the sagittal plane. **(c)** MIP projection of the FMT signal in the transverse plane appears as a transparency color image on a white volume section. This joint showed the strongest reconstructed signal intensity among all healthy joints examined in our study.

the MR findings in terms of relative signal distribution in the transverse plane. The conspicuous signal components appeared in almost the same locations (with respect to anatomic markers) in the transverse plane for both MR and FMT reconstructions. Imperfections were present in FMT reconstructions, as well. The reconstructed fluorescence images are likely to contain strong components at the dorsal side. These components are likely to be attributable to dorsal veins or can be regarded as artifacts. Moreover, the spatial profile of reconstructed fluorescence signal might differ slightly from the synovitis profile seen on the MR image. Such artifacts and reconstruction imperfections are common and understandable in fluorescence tomography and occur even in controlled experiments with homogeneous phantoms (see Appendix E3 [online]). Therefore, the spatial correlation between MR and FMT signal profiles for the results presented here can be reasonably deemed satisfactory and relatively accurate, given the ill-posed nature of the FMT problem and the high levels of modeling imperfection due to lack of complete optical description of in vivo joint tissue. The application of anatomic priors, such as location of bones, obtained from MR images with or without contrast agent or computed tomography (CT), in conjunction with optical measurements, can potentially improve the imaging accuracy, as has already been demonstrated in preclinical application (32). Anatomic images of a given joint can be used to improve the imaging quality of one scan or subsequent FMT scans, through provision of a priori information in the forward modeling or inversion. A similar approach has been used in the study of Yuan et al (6) to improve the accuracy of diffuse optical tomographic imaging of osteoarthritis in distal interphalangeal joints through extraction of anatomic priors from radiography images. Tomographic imaging of synovitis by using FMT can potentially be improved by using higher-order approximations of radiation transport equation instead of the diffusion approximation for modeling light propagation in joint tissue (7).

On the basis of the results presented in our study, all of the healthy joints had a lower signal intensity value (in terms of both mean and maximum intensity) than the ones affected with RA. Joint number 8, which had moderate synovitis at MR imaging, had the strongest fluorescence signal intensity among all joints. This could be caused by the difference in distribution patterns of ICG and MR contrast agent or the experimental variabilities that are unaccounted for. Nevertheless, the proposed method achieved significant signal intensity differences between healthy and inflamed joints. This was shown by performing the two-sided t test on the mean values of reconstructed signal in the MIP ROI, yielding a P value of less than .001. Our data do not provide evidence against the normality assumption in both groups (healthy and affected), as data are distributed symmetrically and no outliers are present. Therefore, use of the two-sided t test

Figure 4

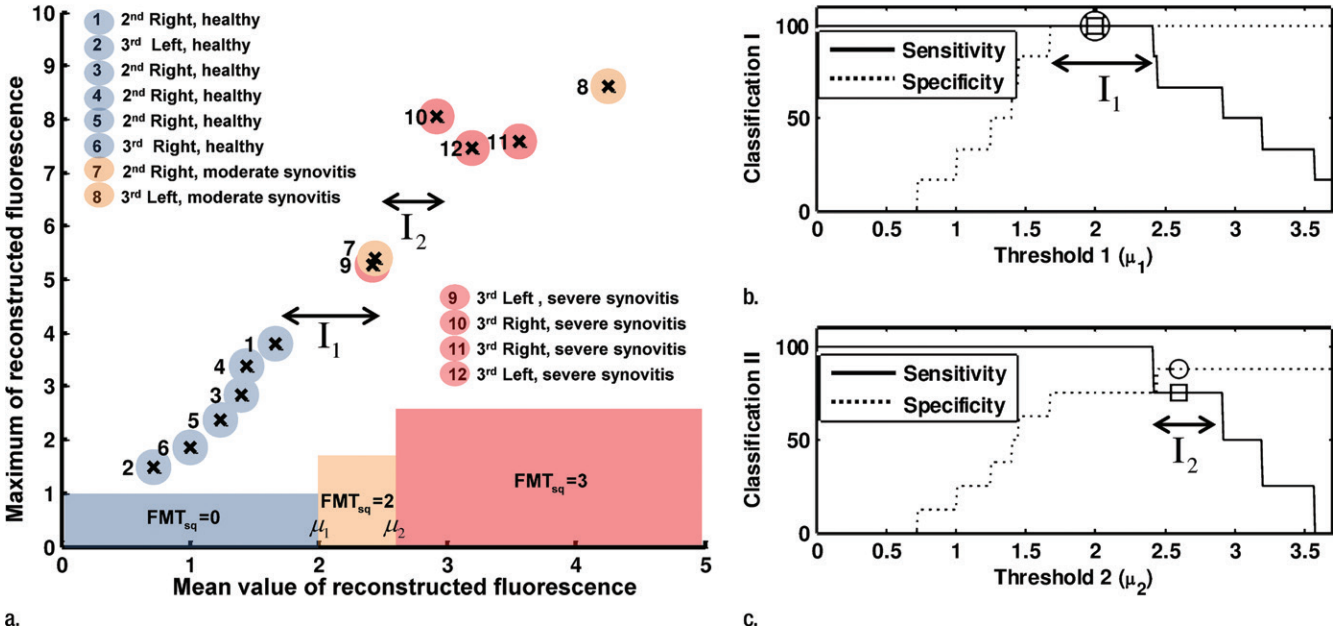

Figure 4: **(a)** Graph shows FMT signal intensity values for the imaged PIP joints of the 12 recruited study participants. Mean versus maximum values of reconstructed fluorescence signal intensity within respective 5-mm MIP ROIs are shown. The blue, orange, and red rectangles show intervals for mean signal intensity values used for FMT semiquantitative scores *(FMT$_{sq}$)* for thresholds $\mu_1 = 2$ and $\mu_2 = 2.6$. Intervals $I_1 = 1.68–2.41$ and $I_2 = 2.45–2.91$ denote ranges for proper setting of μ_1 and μ_2, respectively. **(b)** Graph shows sensitivity (solid line) and specificity (dotted line) for distinguishing between healthy and affected joints (classification I) by using threshold μ_1. The values for $\mu_1 = 2.0$, as used for semiquantitative scoring of FMT signals in **a**, are shown with square and circle markers. Classification I shows the same performance for $\mu_1 \in I_1$. **(c)** Graph shows corresponding results for distinguishing between severe and less-than-severe inflammation (classification 2) by using threshold μ_2. Sensitivity and specificity values for $\mu_2 = 2.6$, as used in **a**, are shown with square and circle makers, respectively. Classification II has the same performance for $\mu_2 \in I_2$. Reconstruction results for subjects 1, 8, and 9 are presented graphically in Figure 3, Figure 2, and Figure E6 (online), respectively.

for comparison of the two groups was justified. As a sensitivity analysis, we also performed a nonparametric test (Mann-Whitney *U* test) that yielded very similar results ($P = .002$).

The increased signal intensity value for the arthritic joints relative to the healthy joints could not be attributed to the higher mean age of the patients. The current data set does not suggest substantial correlation between age and signal intensity values of our study participants (Spearman $\rho = 0.24$). Negative correlation was observed for the available data within patient or volunteer groups ($\rho = -0.77$ for volunteers and $\rho = -0.43$ for patients). A negative correlation value suggests stronger signal intensity for younger study participants. Therefore, the current data set does not suggest the stronger signal intensity in the patients to be an effect of their relatively higher age. In fact, the strongest signal intensity among the patients was measured for the youngest patient (subject 8, aged 41.3 years), and the strongest signal intensity among the volunteers was measured for the second youngest volunteers (subject 1, aged 27.6 years). As another observation, the mean signal intensity value among the older volunteers (subjects 5 and 6, aged 61.2 and 72.8 years, respectively) was 1.12, which is lower than the mean signal intensity among the other four younger volunteers (mean age, 28.8 years; mean signal intensity, 1.31). Similarly, the distribution of signal intensity values for the men in comparison to the women in the current cohort does not hint toward an effect of patient sex on the signal intensity value.

It is not foreseen that FMT will replace MR imaging in the clinic for arthritis imaging. However, owing to its low cost and high sensitivity, FMT is a potential complementary tool for early inflammation detection. The FMT system used in our study is a prototype system with a manufacturing cost of less than 100 000 euros. This cost is an order of magnitude less than the acquisition cost of a clinical MR imaging system, which nominally costs between 1 and 3 million euros. The lower cost of FMT can be attributed to its less expensive components. The most expensive system component of FMT is the cooled charge-coupled–device camera (Pixis 512B; Princeton Instruments). Coregistration of FMT data with MR imaging or CT may allow for precise anatomic orientation and additional information on bone erosions. Further optimization of system hardware and software geared toward faster imaging of all finger joints at lower injection doses is possible and a topic of ongoing research.

Our study has several limitations. The first limitation concerns the relatively long acquisition time of 12 minutes, on average. A large portion of this acquisition time is caused by mechanical and software overheads (Appendix E2 [online]). Second, owing to mechanical difficulties, it was not possible with the current FMT system and holder to image distal interphalangeal joints. Imaging of metacarpophalangeal and carpal joints, which are frequently involved in RA, was not possible with our system because of its current gantry opening size. An FMT system with a larger gantry fully customized for imaging finger joints can potentially address both of these limitations by enabling imaging of other joints and reducing the acquisition times. Third, similar to contrast-enhanced MR imaging, our method requires injection of a contrast agent—namely, the Food and Drug Administration–approved ICG, a fact that may complicate routine application of the proposed method for screening and early detection of RA. The fluorescence was observed to have a nonnegligible value, even up to 1 hour after injection. This fact suggests that it is possible to reduce ICG injection dose—perhaps as low as 0.1 mg per kilogram, as used in the planar RA imaging study presented by Meier et al (4). Fourth, the thresholds μ_1 and μ_2 used for conversion of FMT signal values to semiquantitative scores were adjusted in our study according to the reconstructed signal values for the 12 study participants. A larger study consisting of joints with all degrees of synovitis (scores 0–3) can also help establish thresholds for semiquantitative scoring of synovitis by using the FMT signal. Finally, the statistical evaluation of our method was limited by the number of participants ($n = 12$) in our study. While a larger-scale study is needed to fully characterize the method, the initial results here are promising and demonstrate the potential of imaging RA with FMT.

In summary, our data show that ICG-enhanced FMT allows for detection and characterization of synovitis in finger joints of patients with RA. Owing to its high sensitivity, FMT is a potential complementary imaging tool for early inflammation detection.

Disclosures of Conflicts of Interest: P.M. No relevant conflicts of interest to disclose. **M.K.** No relevant conflicts of interest to disclose. **K.T.** No relevant conflicts of interest to disclose. **B.H.** No relevant conflicts of interest to disclose. **E.J.R.** No relevant conflicts of interest to disclose. **V.N.** No relevant conflicts of interest to disclose. **R.M.** Financial activities related to the present article: none to disclose. Financial activities not related to the present article: author received money from Deutscher Psoriasis Bund and Biogen Idec. Other relationships: None to disclose.

References

1. Quinn MA, Emery P. Window of opportunity in early rheumatoid arthritis: possibility of altering the disease process with early intervention. Clin Exp Rheumatol 2003;21(5,Suppl 31):S154–S157.
2. Backhaus M, Kamradt T, Sandrock D, et al. Arthritis of the finger joints: a comprehensive approach comparing conventional radiography, scintigraphy, ultrasound, and contrast-enhanced magnetic resonance imaging. Arthritis Rheum 1999;42(6):1232–1245.
3. Wakefield RJ, O'Connor PJ, Conaghan PG, et al. Finger tendon disease in untreated early rheumatoid arthritis: a comparison of ultrasound and magnetic resonance imaging. Arthritis Rheum 2007;57(7):1158–1164.
4. Meier R, Thürmel K, Moog P, et al. Detection of synovitis in the hands of patients with rheumatologic disorders: diagnostic performance of optical imaging in comparison with magnetic resonance imaging. Arthritis Rheum 2012;64(8):2489–2498.
5. Hielscher AH, Kim HK, Montejo LD, et al. Frequency-domain optical tomographic imaging of arthritic finger joints. IEEE Trans Med Imaging 2011;30(10):1725–1736.
6. Yuan Z, Zhang Q, Sobel ES, Jiang H. Image-guided optical spectroscopy in diagnosis of osteoarthritis: a clinical study. Biomed Opt Express 2010;1(1):74–86.
7. Hielscher AH, Klose AD, Scheel AK, et al. Sagittal laser optical tomography for imaging of rheumatoid finger joints. Phys Med Biol 2004;49(7):1147–1163.
8. Meier R, Thuermel K, Noël PB, et al. Synovitis in patients with early inflammatory arthritis monitored with quantitative analysis of dynamic contrast-enhanced optical imaging and MR imaging. Radiology 2014;270(1):176–185.
9. Mohajerani P, Meier R, Noël PB, Rummeny EJ, Ntziachristos V. Spatiotemporal analysis for indocyanine green-aided imaging of rheumatoid arthritis in hand joints. J Biomed Opt 2013;18(9):097004.
10. Scheel AK, Krause A, Rheinbaben IM, et al. Assessment of proximal finger joint inflammation in patients with rheumatoid arthritis, using a novel laser-based imaging technique. Arthritis Rheum 2002;46(5):1177–1184.
11. Gu X, Ren K, Hielscher AH. Frequency-domain sensitivity analysis for small imaging domains using the equation of radiative transfer. Appl Opt 2007;46(10):1624–1632.
12. Sun Y, Sobel ES, Jiang H. First assessment of three-dimensional quantitative photoacoustic tomography for in vivo detection of osteoarthritis in the finger joints. Med Phys 2011;38(7):4009–4017.
13. Ntziachristos V. Going deeper than microscopy: the optical imaging frontier in biology. Nat Methods 2010;7(8):603–614.
14. Ntziachristos V, Ripoll J, Wang LV, Weissleder R. Looking and listening to light: the evolution of whole-body photonic imaging. Nat Biotechnol 2005;23(3):313–320.
15. Ntziachristos V, Yodh AG, Schnall M, Chance B. Concurrent MRI and diffuse optical tomography of breast after indocyanine green enhancement. Proc Natl Acad Sci U S A 2000;97(6):2767–2772.
16. Corlu A, Choe R, Durduran T, et al. Three-dimensional in vivo fluorescence diffuse optical tomography of breast cancer in humans. Opt Express 2007;15(11):6696–6716.
17. Intes X, Ripoll J, Chen Y, Nioka S, Yodh AG, Chance B. Diffuse optical tomography of breast with non-specific contrast agent. Philadelphia, Pa: Institute of Electrical and Electronics Engineers, 2002; 87–88.
18. Culver JP, Choe R, Holboke MJ, et al. Three-dimensional diffuse optical tomography in the parallel plane transmission geometry: evaluation of a hybrid frequency domain/continuous wave clinical system for breast imaging. Med Phys 2003;30(2):235–247.
19. Habermehl C, Schmitz CH, Steinbrink J. Contrast enhanced high-resolution diffuse optical tomography of the human brain using ICG. Opt Express 2011;19(19):18636–18644.
20. Herzog E, Taruttis A, Beziere N, Lutich AA, Razansky D, Ntziachristos V. Optical imaging of cancer heterogeneity with multispectral optoacoustic tomography. Radiology 2012;263(2):461–468.
21. Buehler A, Herzog E, Razansky D, Ntziachristos V. Visualization of mouse kidney perfusion with multispectral optoacoustic tomography (MSOT) at video rate. In: Oraevsky AA, Wang LV, eds. Proceedings of SPIE: photons plus ultrasound: imaging and sensing 2011. Vol 7899. Bellingham, Wash:

SPIE–The International Society for Optical Engineering, 2011; 789914.

22. Cuccia DJ, Bevilacqua F, Durkin AJ, et al. In vivo quantification of optical contrast agent dynamics in rat tumors by use of diffuse optical spectroscopy with magnetic resonance imaging coregistration. Appl Opt 2003;42(16):2940–2950.

23. Gulsen G, Yu H, Wang J, et al. Congruent MRI and near-infrared spectroscopy for functional and structural imaging of tumors. Technol Cancer Res Treat 2002;1(6):497–505.

24. Meier R, Krug C, Golovko D, et al. Indocyanine green-enhanced imaging of antigen-induced arthritis with an integrated optical imaging/radiography system. Arthritis Rheum 2010;62(8):2322–2327.

25. Østergaard M, Peterfy C, Conaghan P, et al. OMERACT Rheumatoid Arthritis Magnetic Resonance Imaging Studies. Core set of MRI acquisitions, joint pathology definitions, and the OMERACT RA-MRI scoring system. J Rheumatol 2003;30(6):1385–1386.

26. Schulz RB, Ale A, Sarantopoulos A, et al. Hybrid system for simultaneous fluorescence and x-ray computed tomography. IEEE Trans Med Imaging 2010;29(2):465–473.

27. Arridge SR, Schweiger M, Hiraoka M, Delpy DT. A finite element approach for modeling photon transport in tissue. Med Phys 1993;20(2 Pt 1):299–309.

28. Soubret A, Ntziachristos V. Fluorescence molecular tomography in the presence of background fluorescence. Phys Med Biol 2006;51(16):3983–4001.

29. Paige CC, Saunders MA. LSQR: An algorithm for sparse linear equations and sparse least squares. TOMS 1982;8(1):43–71.

30. Bugbee WD, Botte MJ. Surface anatomy of the hand. The relationships between palmar skin creases and osseous anatomy. Clin Orthop Relat Res 1993 (296):122–126.

31. Fleiss JL, Levin B, Paik MC. Statistical methods for rates and proportions. New York, NY: Wiley, 2013.

32. Ale A, Ermolayev V, Herzog E, Cohrs C, de Angelis MH, Ntziachristos V. FMT-XCT: in vivo animal studies with hybrid fluorescence molecular tomography-X-ray computed tomography. Nat Methods 2012;9(6):615–620.

33. Clarke TA, Fryer JG. The development of camera calibration methods and models. Photogramm Rec 1998;16(91):51–66.

34. Fang Q, Boas DA. Tetrahedral mesh generation from volumetric binary and gray-scale images. In: IEEE International Symposium on Biomedical Imaging: From Nano to Macro, 2009. ISBI '09. Vols 1 and 2. Piscataway, NJ: Institute of Electrical and Electronics Engineers, 2009; 1142–1145.